JOURNAL OF COMPUTATIONAL PHYSICS 84, 343–359 (1989)

Boundary Value Problems in Magnetohydrodynamics (and Fluid Dynamics). I. Radiation Boundary Condition

T. C. VANAJAKSHI, KEVIN W. THOMPSON, AND DAVID C. BLACK

Space Science Division, NASA Ames Research Center, Moffett Field, California 94035

Received February 26, 1988; revised December 9, 1988

Numerical simulations of time-dependent phenomena involving magnetohydrodynamic (MHD) waves encounter serious problems due to artificial reflection of waves at numerical boundaries in situations where the time-dependent magnetic fields external to those boundaries are not known. A method developed for determining radiative (i.e., nonreflecting) boundary conditions for waves in ordinary fluids is generalized in this paper to treat isothermal MHD waves. A test problem is considered for which analytic results have been obtained, namely, magnetic braking of a rigidly rotating disk embedded in a differentially rotating fluid. Comparison is made between results obtained from numerical simulations, with and without the radiative boundary treatment developed here, and the analytic results. © 1989 Academic Press, Inc.

1. INTRODUCTION

One of the difficulties encountered in numerical simulations of problems which involve no physical boundaries (many problems in astrophysics) is the determination of the field components and material velocities at the boundary of the calculation. Such determinations often require information from outside the numerical grid. Fixing the values of these variables artificially at computational boundaries causes spurious reflection of wave-related properties (e.g., the energy) back into the numerical grid. This can eventually affect the results in the interior of the numerical grid enough to make them unreliable. A method has been developed by Thompson [1] for nonreflecting boundary conditions, in the case of multi-dimensional inviscid fluid dynamics. This approach uses the methd of characteristics to separate the incoming and outgoing waves and then selectively suppresses the incoming modes. In this paper the method has been extended to handle multi-dimensional magnetohydrodynamic (MHD) waves. The results of a 2D case which can be solved analytically (for comparison) are presented. The simulation uses a cylindrical coordinate grid. In Section 3 the equations for a full 3D simulation of the motion of a compressible, magnetic, nonviscous fluid are given and the application of the radiation boundary condition for this most general case is described. In Section 4 the 2D example is described in detail and the results are presented in Section 5.

0021-9991/89 $3.00

2. Physical Equations

In a full 3D system the motion of a compressible, isothermal, non-viscous, perfectly conducting fluid in the presence of a magnetic field is described by:

Equation of mass conservation (continuity equation):

$$\frac{\partial \rho}{\partial t} + \nabla \cdot (\rho \mathbf{v}) = 0; \tag{1}$$

Equation of momentum conservation:

$$\rho \frac{\partial \mathbf{v}}{\partial t} + \rho(\mathbf{v} \cdot \nabla)\mathbf{v} = -\nabla p - \nabla \Phi - \frac{1}{4\pi} \mathbf{B} \times (\nabla \times \mathbf{B}) \tag{2}$$

Equation of magnetic flux conservation (induction equation):

$$\frac{\partial \mathbf{B}}{\partial t} = \nabla \times (\mathbf{v} \times \mathbf{B}), \tag{3}$$

supplemented by the equation of state:

$$p = c^2 \rho \qquad \text{(isothermal gas)}. \tag{4}$$

The detailed equations in primitive form are given in the Appendix.

3. The Radiation Boundary Condition

The basic approach of non-reflecting boundary conditions in time-dependent problems for non-MHD waves is described in Thompson [1]. The principles are applied here to the full set of equations given in Section 2. The following approach is based on the properties of waves in one dimension. While we have no formal proof that this technique is valid in problems with more than one spatial dimension it seems to work well in many cases of interest, as shown in [1].

3.1. *Description of the Radiation Boundary Condition*

The boundary conditions to be developed make use of the primitive form of the equations (as given in the Appendix), rather than the conservative form, in order to simplify the characteristic analysis below. The following analysis assumes that the equations are to be solved in cylindrical geometry (coordinates r, ϕ, and z), for the primitive variables ρ, u, v, w, B_r, B_ϕ, and B_z, as in the Appendix. The non-reflecting boundary conditions must be applied in both the r and z directions. The general approach taken is as follows.

Let **U** be the vector of dependent variables in the primitive system. The system of equations is represented (in cylindrical coordinates) by

$$\frac{\partial \mathbf{U}}{\partial t} + \mathbf{A}\frac{\partial \mathbf{U}}{\partial r} + \mathbf{B}\frac{\partial \mathbf{U}}{\partial z} + \mathbf{C} = 0, \tag{5}$$

where **A** and **B** are $n \times n$ coefficient matrices and **C** is a column vector of length n which contains all non-derivative (inhomogeneous) terms.

If we *define* the quantities $(\partial \mathbf{U}/\partial t)_r$ and $(\partial \mathbf{U}/\partial t)_z$ by

$$\left(\frac{\partial \mathbf{U}}{\partial t}\right)_r + \mathbf{A}\frac{\partial \mathbf{U}}{\partial r} = 0, \qquad \left(\frac{\partial \mathbf{U}}{\partial t}\right)_z + \mathbf{B}\frac{\partial \mathbf{U}}{\partial z} = 0, \tag{6}$$

then Eq. (5) may be written as

$$\frac{\partial \mathbf{U}}{\partial t} = \left(\frac{\partial \mathbf{U}}{\partial t}\right)_r + \left(\frac{\partial \mathbf{U}}{\partial t}\right)_z - \mathbf{C}. \tag{7}$$

The evaluation of $\partial \mathbf{U}/\partial t$ at a boundary in the r direction, say at the outer boundary $r = r_{\max}$, is non-trivial, as the terms represented by $(\partial \mathbf{U}/\partial t)_r$ contain derivatives in the r direction and generally require data exterior to the grid for their evaluation. We therefore make use of characteristic analysis to determine which contributions to $(\partial \mathbf{U}/\partial t)_r$ may be evaluated from data within the grid, and we impose a non-reflecting boundary condition to determine the remaining contributions and close the system of equations.

The contributions to $\partial \mathbf{U}/\partial t$ from $(\partial \mathbf{U}/\partial t)_z$ and **C** at the r boundaries do not involve derivatives in the r direction and consequently involve data already present on the grid. They are computed just as in the interior of the grid. A similar approach is taken at the z boundaries, which will therefore not be discussed explicitly. We will focus on the evaluation at the r boundaries of $(\partial \mathbf{U}/\partial t)_r$.

Note that this partitioning of terms into normal and transverse directions at the boundaries implies that the boundaries lie along constant-coordinate surfaces. Boundaries which do not satisfy this condition may be dealt with by performing a coordinate transformation of the differential equations which aligns the boundary with a new coordinate surface.

We begin by evaluating $(\partial \mathbf{U}/\partial t)_r$ as given by

$$\left(\frac{\partial \mathbf{U}}{\partial t}\right)_r + \mathbf{A}\frac{\partial \mathbf{U}}{\partial r} = 0. \tag{8}$$

Following the procedure in [1], we first compute the eigenvalues and eigenvectors of the coefficient matrix **A**. The eigenvalues λ_i of **A**, conventionally ordered so that $\lambda_1 \leqslant \lambda_2 \leqslant \cdots \leqslant \lambda_n$, represent the characteristic velocities at which the

different wave modes propagate. If $\boldsymbol{l}_i$ and $\mathbf{r}_i$ are the left and right eigenvectors of $\mathbf{A}$, satisfying

$$\boldsymbol{l}_i^{\mathrm{T}}\mathbf{A} = \lambda_i \boldsymbol{l}_i^{\mathrm{T}}, \qquad \mathbf{A}\mathbf{r}_i = \lambda_i \mathbf{r}_i, \tag{9}$$

(where $\boldsymbol{l}_i^{\mathrm{T}}$ is the transpose of $\boldsymbol{l}_i$), then Eq. (8) may be written

$$\boldsymbol{l}_i^{\mathrm{T}}\left(\frac{\partial \mathbf{U}}{\partial t}\right)_r + \lambda_i \boldsymbol{l}_i^{\mathrm{T}}\frac{\partial \mathbf{U}}{\partial r} = 0, \tag{10}$$

or

$$\boldsymbol{l}_i^{\mathrm{T}}\left(\frac{\partial \mathbf{U}}{\partial t}\right)_r + \mathscr{L}_i = 0, \qquad \mathscr{L}_i \equiv \lambda_i \boldsymbol{l}_i^{\mathrm{T}}\frac{\partial \mathbf{U}}{\partial r}. \tag{11}$$

At the boundary $r = r_{\max}$, wave modes for which $\lambda_i > 0$ are propagating out of the model, and $\mathscr{L}_i$ may be computed from its definition in (11) by using one-sided finite difference approximations to $\partial \mathbf{U}/\partial r$, using only interior data. (Similarly, at $r = r_{\min}$ we may compute $\mathscr{L}_i$ from its definition in (10) when $\lambda_i < 0$, using one-sided differences, as this case also corresponds to an outgoing wave.)

However, if $\lambda_i < 0$ for some modes, then those waves are propagating into the model and generally may not be computed from interior data. In this case we make use of the *nonreflecting boundary condition* of Ref. [1] and set $\mathscr{L}_i = 0$ (and set $\mathscr{L}_i = 0$ at the inner boundary if $\lambda_i > 0$), which may be done conveniently by replacing λ_i by 0 in the definition of $\mathscr{L}_i$.

We may also define a similarity transformation for the matrix $\mathbf{A}$ which generates the characteristic form of the wave equations. Let

$$\mathbf{S}^{-1}\mathbf{A}\mathbf{S} = \boldsymbol{\Lambda}, \tag{12}$$

where the columns of $\mathbf{S}$ are the right eigenvectors $\mathbf{r}_i$, the rows of $\mathbf{S}^{-1}$ are the left eigenvectors $\boldsymbol{l}_i$, and $\boldsymbol{\Lambda}$ is the diagonal matrix of eigenvalues, with $\Lambda_{ii} = \lambda_i$. This definition of $\mathbf{S}$ in terms of eigenvectors assumes a normalized, bi-orthogonal set of vectors satisfying $\boldsymbol{l}_i^{\mathrm{T}} \cdot \mathbf{r}_j = \delta_{ij}$. Multiplying Eq. (8) from the left by $\mathbf{S}^{-1}$ gives

$$\mathbf{S}^{-1}\left(\frac{\partial \mathbf{U}}{\partial t}\right)_r + \boldsymbol{\Lambda}\mathbf{S}^{-1}\frac{\partial \mathbf{U}}{\partial r} = 0, \tag{13}$$

which is the complete set of wave equations.

The nonreflecting boundary conditions are implemented in the form of Eq. (13) by replacing the matrix $\boldsymbol{\Lambda}$ by $\boldsymbol{\Lambda}'$, where $\Lambda'_{ii} = \lambda_i$ for outgoing waves, and $\Lambda'_{ii} = 0$ otherwise.

Given the set of simultaneous equations for the time derivatives $(\partial U_i/\partial t)_r$, in the form of (13), we then solve for the time derivatives and integrate them to obtain the unknowns at the next time step. The solution of (13) may be performed analytically or numerically. Analytic solutions are generally preferable, both from the standpoint of speed and accuracy. Difficulties may arise in the numerical solution if the matrix $\mathbf{S}^{-1}$ is nearly singular.

The most robust solution technique we have found to date relies on a numerical solution for the eigenvectors of a modified (symmetrized) version of the matrix **A**, and then takes advantage of the orthogonality of the left and right eigenvectors of the symmetric matrix to obtain the solution for the time derivatives. While an analytic solution for the eigenvectors would be preferable, it involves special conditions to be specified for every possible configuration of zero and nonzero magnetic field components. The degree of degeneracy of the eigenvalues changes as the different field components vanish, leading to a very complicated set of equations for the eigenvectors. This problem is avoided by using the semi-analytic approach described below.

3.2. *Description of the Semi-analytic Approach*

The solution process is greatly simplified if it is possible to introduce a symmetric matrix $\mathbf{A}'$, which is obtained from **A** by the similarity transformation

$$\mathbf{A}' \equiv \mathbf{D}^{-1}\mathbf{A}\mathbf{D}, \tag{14}$$

where **D** is the diagonal matrix that symmetrizes **A**.

The eigenvectors (left or right) of **A** will always be linearly independent, but they are not orthogonal, and it is possible that any two of them may be nearly parallel. Consequently the matrix $\mathbf{S}^{-1}$ may be ill-conditioned, i.e., so nearly singular that the numerical solution of Eq. (13) is poorly determined. In contrast, the eigenvectors of the symmetric matrix $\mathbf{A}'$ are orthogonal (as is the case for any symmetric matrix), and not only lead to a well-conditioned set of linear equations, but allow an analytic solution to the equations. The symmetry of the matrix and the orthogonality of the eigenvectors make the numerical determination of the eigenvectors of $\mathbf{A}'$ more accurate as well.

We now have

$$\mathbf{A}'\mathbf{G} = \mathbf{G}\Lambda, \tag{15}$$

where **G** is the matrix of right eigenvectors of the symmetrized matrix $\mathbf{A}'$. If the right eigenvectors are normalized to have unit modulus, then the transpose of **G** is the same as its inverse, and is the matrix of left eigenvectors; hence

$$\mathbf{D}^{-1}\mathbf{A}\mathbf{D} = \mathbf{G}\Lambda\mathbf{G}^{\mathrm{T}}. \tag{16}$$

The equation $(\partial\mathbf{U}/\partial t)_r + \mathbf{A}\cdot\partial\mathbf{U}/\partial r = 0$ can be transformed to yield a set of equations which can be solved in a straightforward manner, as shown below:

$$\mathbf{D}^{-1}\left(\frac{\partial \mathbf{U}}{\partial t}\right)_r + \mathbf{D}^{-1}\mathbf{A}\frac{\partial \mathbf{U}}{\partial r} = 0, \tag{17}$$

$$\left(\frac{\partial \mathbf{U}}{\partial t}\right)_r = -\mathbf{D}(\mathbf{G}\Lambda\mathbf{G}^{\mathrm{T}})\mathbf{D}^{-1}\frac{\partial \mathbf{U}}{\partial r}. \tag{18}$$

We now have an explicit solution for $(\partial\mathbf{U}/\partial t)_r$.

The eigenvector matrix **G** for the MHD problem is obtained numerically, as are the eigenvalues λ_i, but the remainder of the calculation in (18) is performed analytically.

If we now replace **A** in (18) by **A**′, then Eq. (18) has the radiative boundary conditions built into it. Because the term on the right-hand side can be evaluated by one-sided differencing, this set of equations can be solved directly for the six variables that constitute the column vector **U**. For a full 3D case along the r boundary,

$$\mathbf{U}=\begin{pmatrix}\rho\\ u\\ v\\ w\\ B_\phi\\ B_z\end{pmatrix},\qquad \mathbf{A}=\begin{pmatrix} u & \rho & 0 & 0 & 0 & 0\\ \dfrac{c^2}{\rho} & u & 0 & 0 & \dfrac{B_\phi}{4\pi\rho} & \dfrac{B_z}{4\pi\rho}\\ 0 & 0 & u & 0 & \dfrac{-B_r}{4\pi\rho} & 0\\ 0 & 0 & 0 & u & 0 & \dfrac{-B_r}{4\pi\rho}\\ 0 & B_\phi & -B_r & 0 & u & 0\\ 0 & B_z & 0 & -B_r & 0 & u\end{pmatrix}, \tag{19}$$

and the symmetrized matrix $\mathbf{A}'$ ($\equiv \mathbf{D}^{-1}\mathbf{A}\mathbf{D}$) is

$$\mathbf{A}'=\begin{pmatrix} u & c & 0 & 0 & 0 & 0\\ c & u & 0 & 0 & \dfrac{B_\phi}{\sqrt{4\pi\rho}} & \dfrac{B_z}{\sqrt{4\pi\rho}}\\ 0 & 0 & u & 0 & \dfrac{-B_r}{\sqrt{4\pi\rho}} & 0\\ 0 & 0 & 0 & u & 0 & \dfrac{-B_r}{\sqrt{4\pi\rho}}\\ 0 & \dfrac{B_\phi}{\sqrt{4\pi\rho}} & \dfrac{-B_r}{\sqrt{4\pi\rho}} & 0 & u & 0\\ 0 & \dfrac{B_z}{\sqrt{4\pi\rho}} & 0 & \dfrac{-B_r}{\sqrt{4\pi\rho}} & 0 & u\end{pmatrix}. \tag{20}$$

The diagonal elements of the symmetrizing matrix **D** and its inverse are:

$$\mathrm{diag}(\mathbf{D})=\left(1,\frac{c}{\rho},\frac{c}{\rho},\frac{c}{\rho},\sqrt{4\pi\rho}\,\frac{c}{\rho},\sqrt{4\pi p}\,\frac{c}{p}\right), \tag{21}$$

$$\mathrm{diag}(\mathbf{D}^{-1})=\left(1,\frac{\rho}{c},\frac{\rho}{c},\frac{\rho}{c},\frac{1}{\sqrt{4\pi\rho}}\,\frac{\rho}{c},\frac{1}{\sqrt{4\pi\rho}}\,\frac{\rho}{c}\right). \tag{22}$$

The basic equations used here ((1)–(3) or (45)–(51)) have been taken in their most general form. As such it can safely be said that the symmetrizability of the matrix and the consequent simplicication of the rest of the approach are likely to be applicable in all problems in isothermal fluid dynamics, both magneto-hydrodynamic and non-magnetohydrodynamic. For other problems with real eigenvalues it may also be possible to symmetrize the initially non-symmetric matrices, though not necessarily by using a diagonal matrix. In the latter case one might choose a different set of dependent variables such that the resultant matrix can be symmetrized easily.

4. Solution of the 2D Case

For the first trial a 2D analytical case studied by Mouschovias [2] was tried. This case involves a cylindrical cloud of uniform density ρ_{cl} with a given initial angular velocity Ω_0 about its axis of symmetry (the z axis), embedded in an initially quiescent external medium of uniform density ρ_{ext}, which is allowed to rotate differentially. A frozen-in magnetic field, initially radial and perpendicular to the (rotation) axis of symmetry radiates out from the cloud into the external medium (see Fig. 1). The angular velocity of the cloud as a function of time is calculated as the rotational energy is converted into magnetic energy and pumped out along the field lines through Alfven waves.

Because of the symmetry of the problem the numerical grid need span only the region $r \geqslant 0$, $z \geqslant 0$. Therefore we are concerned only with the boundary along the $+r$ direction. Because of the radial field geometry the reflection along the z boundary does not arise.

The assumption of cylindrical symmetry and flux freezing along with the constraint $\nabla \cdot \mathbf{B} = 0$, which applies for all the magnetic fields at all times, gives rise to the following set of equations for the time evolution of the magnetic field and the angular velocity of the cloud and the external medium (Mouschovias [2]):

(a) External medium:

$$\frac{\partial B_\phi(r, t)}{\partial t} = RB_0 \frac{\partial \Omega(r, t)}{\partial r} \tag{23}$$

$$\frac{\partial \Omega(r, t)}{\partial t} = \frac{RB_0}{4\pi\rho_{ext} r^3} \frac{\partial (rB_\phi)}{\partial r} \tag{24}$$

(Mouschovias [2, Eq. (7), (10)]). Here R is the radius of the cloud and B_0 the value of the magnetic field at the cloud surface at $t = 0$. The external medium is allowed to rotate differentially but there is no material exchange across the cloud surface or across the external medium.

(b) Cloud:

$$\frac{\partial \Omega_{cl}(t)}{\partial t} = \frac{B_0}{\rho_{cl} \pi R^2} B_\phi(r, t) \tag{25}$$

(for details see [2]).

When solving this problem numerically the finite grid structure puts an artificial limit on the extent of the external medium (in the analytical approach it can be assumed to be infinite). This creates problems in the determination of the magnetic fields along the boundary, which needs information from regions external to the boundary. Any ad hoc approximations to the **B** field create a spurious, reflected Alfven wave. This wave eventually reaches the cloud and spins it up. Application

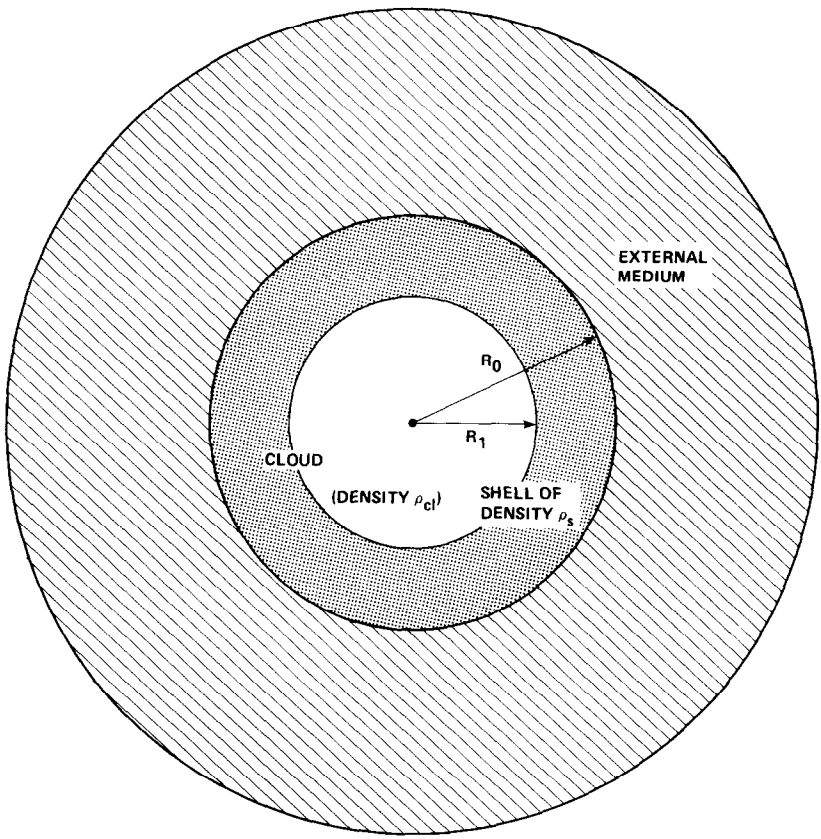

FIG. 1. Schematic diagram of cloud represented as a shell with equivalent moment of inertia.

of the radiation boundary condition eliminates this problem as the results in Section 4 show.

4.1. *Application of Radiation Boundary Condition to the 2D Model*

In this case, we are concerned only with the outer r boundary, and the vector $\mathbf{U}$ is a column vector with just two elements:

$$\mathbf{U} = \begin{pmatrix} B_\phi \\ \Omega \end{pmatrix}. \tag{26}$$

The two relevant equations are,

$$\frac{\partial B_\phi}{\partial t} = RB_0 \frac{\partial \Omega}{\partial r}, \tag{27}$$

$$\frac{\partial \Omega}{\partial t} - \beta r \frac{\partial B_\phi}{\partial r} - \beta B_\phi = 0, \qquad \beta \equiv \frac{RB_0}{4\pi \rho_{\text{ext}} r^3}. \tag{28}$$

In matrix form

$$\mathbf{U} = \begin{pmatrix} B_\phi \\ \Omega \end{pmatrix}, \qquad \mathbf{A} = \begin{pmatrix} 0 & -RB_0 \\ -\beta r & 0 \end{pmatrix}, \qquad \mathbf{C} = \begin{pmatrix} 0 \\ -\beta B\phi \end{pmatrix}. \tag{29}$$

Since these equations are simple we carry the $\mathbf{C}$ term along instead of splitting the equation into the two parts (as in $\partial \mathbf{U}/\partial t = (\partial \mathbf{U}/\partial t)_r - \mathbf{C}$). Thus the two equations (27) and (28) are combined into the form

$$\frac{\partial \mathbf{U}}{\partial t} + \mathbf{A} \frac{\partial \mathbf{U}}{\partial r} + \mathbf{C} = 0. \tag{30}$$

The eigenvalues of $\mathbf{A}$ (the characteristic velocities) are

$$\lambda_1 = -\sqrt{\beta RB_0 r}, \qquad \lambda_2 = \sqrt{\beta RB_0 r}. \tag{31}$$

At the outer radial boundary λ_1 corresponds to the reflected wave and λ_2 represents the outward travelling wave. As this is a fairly simple problem, we can obtain the eigenvectors of $\mathbf{A}$ analytically and do not need to set up a numerically well-conditioned problem; consequently we do not apply the additional transformations described in Section 3 for the 3D case.

The left eigenvectors $\boldsymbol{l}_i$ can be calculated from the equation

$$\boldsymbol{l}_i^{\mathrm{T}} \mathbf{A} = \lambda_i \boldsymbol{l}_i^{\mathrm{T}}. \tag{32}$$

Thus

$$l_{12} = \sqrt{\frac{RB_0}{\beta r}}\, l_{11}, \qquad l_{11} \text{ is arbitrary}, \tag{33}$$

$$l_{22} = -\sqrt{\frac{RB_0}{\beta r}}\, l_{21}, \qquad l_{21} \text{ is arbitrary,} \tag{34}$$

$$\boldsymbol{l}_1 = (\sqrt{\beta r}, \sqrt{RB_0}), \qquad \boldsymbol{l}_2 = (\sqrt{\beta r}, -\sqrt{RB_0}). \tag{35}$$

We now have

$$\boldsymbol{l}_i^{\mathrm{T}} \frac{\partial \mathbf{U}}{\partial t} + \lambda_i \boldsymbol{l}_i^{\mathrm{T}} \frac{\partial \mathbf{U}}{\partial r} + \boldsymbol{l}_i^{\mathrm{T}} \mathbf{C} = 0. \tag{36}$$

Written out in full, Eq. (36) is

$$\sqrt{\beta r}\frac{\partial B_\phi}{\partial t} + \sqrt{RB_0}\frac{\partial \Omega}{\partial t} + \lambda_1\left(\sqrt{\beta r}\frac{\partial B_\phi}{\partial r} + \sqrt{RB_0}\frac{\partial \Omega}{\partial r}\right) - \sqrt{RB_0}\,\beta B_\phi = 0, \tag{37}$$

$$\sqrt{\beta r}\frac{\partial B_\phi}{\partial t} - \sqrt{RB_0}\frac{\partial \Omega}{\partial t} + \lambda_2\left(\sqrt{\beta r}\frac{\partial B_\phi}{\partial r} - \sqrt{RB_0}\frac{\partial \Omega}{\partial r}\right) + \sqrt{RB_0}\,\beta B_\phi = 0. \tag{38}$$

Since λ_1, which is negative, corresponds to the reflected wave along the positive r direction, application of the radiation boundary condition requires setting $\mathscr{L}_1$ to zero. Therefore Eq. (37) becomes

$$\sqrt{\beta r}\frac{\partial B_\phi}{\partial t} + \sqrt{RB_0}\frac{\partial \Omega}{\partial t} - \sqrt{RB_0}\,\beta B_\phi = 0, \tag{39}$$

while Eq. (38) remains the same.

These two simultaneous equations can be solved to give $\partial B_\phi/\partial t$ and $\partial \Omega/\partial t$. The new values of the variables B_ϕ and Ω are obtained by integrating the time derivatives, as in

$$\mathbf{U}^{n+1} = \mathbf{U}^n + \Delta t \cdot \frac{\partial \mathbf{U}}{\partial t}. \tag{40}$$

4.2. *Details of the Calculation*

It is important to be able to verify numerical schemes through comparison with either data or with results obtained from analytic calculations. We were able to use the analytic results of Mouschovias [2] as the basis for verification of the numerical approach developed here. In order to achieve the accuracy obtained in the analytical calculations of Mouschovias [2] very fine-resolution computational grids were used near the interface of the cloud and the external medium. This severely restricted the size of the time steps due to the Courant condition for the stability of the explicit finite difference approach. Consequently the later part of the time evolution of the system required a significant amount of computer time. For this reason we elected to compare our results with those of Mouschovias only over the first 0.5 Alfven crossing times. That comparison is given in Fig. 2. Therefore once

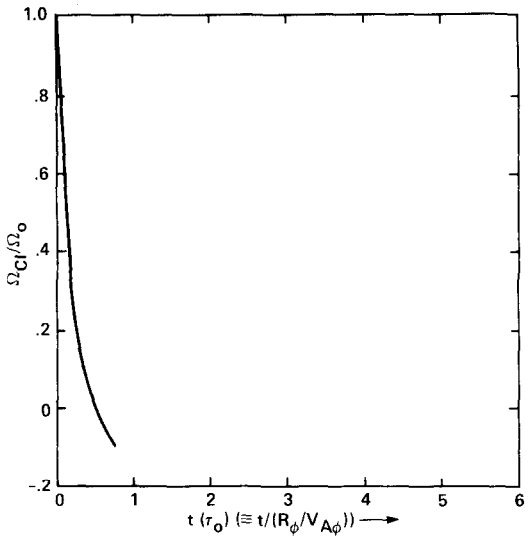

FIG. 2. Angular momentum of cloud as a function of time—fine-grid resolution.

we had confirmed that the code produced accurate results with this small grid spacing we increased the grid spacing and performed the simulations to larger times. Once the cell size was made larger the time evolution of the system slowed and the angular momentum evolution of the cloud lagged behind that of Mouschovias. Three sets of runs were completed:

1. The first run was performed without the reflection boundary condition for purposes of comparison (curve 1, Fig. 3).

2. The second was a run with the nonreflecting boundary condition in force (curve 2, Fig. 3).

3. The third was performed with the external medium 3 times as large as for the previous runs so that reflection did not occur during the time scale of the run (curve 3, Fig. 3).

In order to simulate this case numerically we used a cylindrical grid structure with 90 grid points in the radial direction. In all runs the cloud occupied the innermost five grid points. This is because, in this situation, the cloud is considered a rigid body with a constant (radial) magnetic field $\mathbf{B}_0$ and all the changes occur from the interface *outwards*. The only cell that is of interest from inside the cloud is the one just inside the cloud boundary forming the interface between the cloud and the external medium. Spatial derivatives at the interface have to take into account the values of the variables at the center of this grid. But all the cells interior to this border cell are irrelevant to the numerical computations. Therefore most of the grid points are dedicated to the external medium. However this approach necessitates certain modifications in the way the cloud is represented, for the following reason:

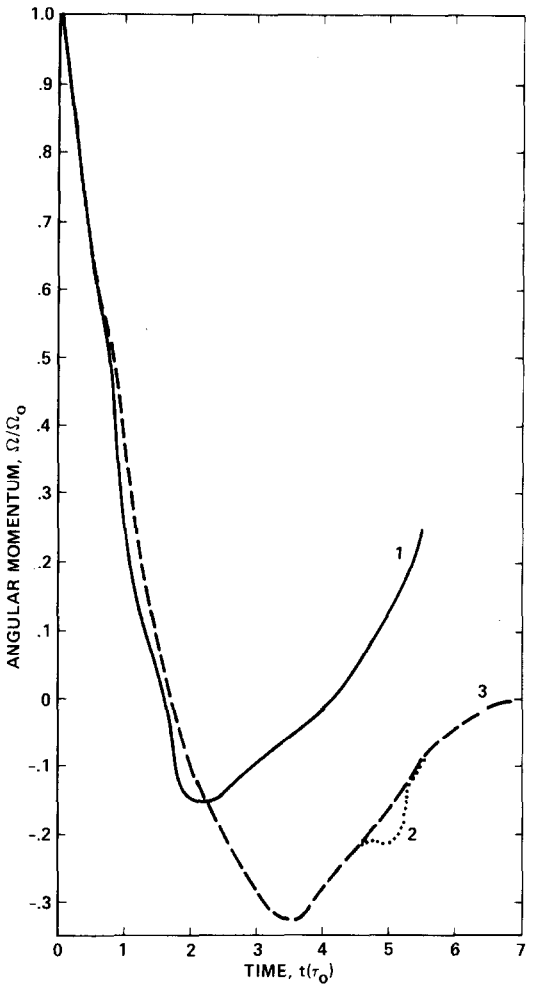

FIG. 3. Angular momentum of cloud as a function of time.

Since there are only five grids inside the cloud, if they are equally, or even geometrically spaced, the width of the border cell will be much larger than that of the cell immediately on the other side of the interface ($\sim 1/90 R_0$ if evenly spaced grids and smaller still if geometric progression is used for the spacing in the external medium). This discrepancy in the widths can cause gross inaccuracy in the results due to uneven spatial derivatives. To avoid this the cells on both sides have to have the same (small) width ΔR. To achieve this and at the same time keep the number of grids small inside the cloud we represented the cloud as a *cylindrical shell* (of different density) whose moment of inertia is the same as that of a rigid sphere of radius R_0 and density ρ_{cl}. (Since there are no variations in the Z-direction the cloud is equivalent to a cylinder stacked with rigid disks with the axis of the

cylinder being the Z-axis of the grid.) This approach also obviates the necessity of artificially redistributing the angular momentum, at each time step, inside the cloud in order to represent rigid body rotation. When configured in this fashion the cloud is represented by this shell for all practical purposes and maintains the accuracy of the calculations. The grids interior to the shell are completely ignored in the computations. This shell can be made as thin as necessary by increasing its density correspondingly. The appropriate density for the shell is calculated from the equation:

$$\rho_{\text{shell}} = \rho_{\text{cloud}} \left(\frac{R_0^4}{R_0^4 - R_1^4} \right). \tag{41}$$

A shematic diagram (Fig. 1) illustrates the concept.

The spacing of the grid points *outside* the cloud, i.e., in the external medium, was computed using geometric progression,

$$\Delta R_{J+1} = \alpha \, \Delta R_J \tag{42}$$

$$R_0 = \sum_{k=0}^{n-1} \alpha^k \, \Delta R_1 = \frac{1-\alpha^n}{1-\alpha} \, \Delta R_1, \tag{43}$$

where n = number of grids in the external medium. From this relation α is calculated using Newton's method. Typical values for α fall in the range 1.0259–1.1425 depending on the number of grid points used. Several different values of ΔR_1 corresponding to different numbers of cells were tried in order to achieve maximum sensitivity near the interface, subject to the limitations posed by numerical accuracy. But the value of α remained constant for every *set* of the three runs referred to earlier. For run 3 we used 270 grid points with the same ratio α as in the other two runs.

This simulation was performed using a full 3D MHD code and we allowed 10 grid points in the Z-direction just to make sure that the code indeed reproduced the results faithfully when there was no variation in the Z-direction and that no instability was introduced by numerical noise for this direction.

5. Results

The results are presented in Fig. 3. It shows the (non-dimensional) angular velocity of the cloud Ω/Ω_0 as a function of time in units of Alfven crossing time τ_0, where

$$\tau_0 = \frac{R_0}{v_{A0}} = \frac{R_0}{B_0 \sqrt{4\pi\rho_{\text{ext}}}}. \tag{44}$$

Curve 1 corresponds to run 1 without the nonreflecting boundary condition. It can be seen that the maximum retrograde motion (negative Ω/Ω_0) is much less (-0.15) than the other two cases (-0.35). This happens because the reflected wave has traveled back to the center by this time and is starting to spin the cloud up in the other direction. As the system evolves further in time the retrograde motion is stopped completely and by four Alfven crossing times the cloud is starting to gain angular momentum in the positive direction and continues to do so as time goes on.

Curve 2 corresponds to the run with the nonreflecting boundary condition in effect and the results are quite different. After reaching a maximum retrograde motion of $\Omega/\Omega_0 = -0.35$ the rotation of the cloud asymptotically tends to zero by about seven Alfven crossing times. Around $4.6\tau_0$ there is a small wiggle in the curve, presumably due to numerical inaccuracies.

Curve 3 corresponds to the run with the extended external medium so that the wave keeps travelling outward for the duration of the simulation. As can be seen from the plot, the two curves 2 and 3 are almost identical except for the numerical noise around $4.6\tau_0$.

We interpret the wiggle in curve 2 at $\sim 5\tau_0$ as numerical noise due to insufficient grid resolution rather than reflection of Alfven waves at the boundary for the following two reasons: (1) Runs corresponding to curve 2 with coarser grids showed similar but larger deviations between curves 2 and 3; (2) If there is reflection its effect should have been observed once the reflected wave reached the cloud boundary. This would have occurred $\sim 1.6\tau_0$ since the wave takes $0.8\tau_0$ to traverse the external medium between the cloud boundary and the outer boundary. An examination of curves 2 and 3 shows that the curves overlap completely for a long time ($\sim 4.5\tau_0$) which is sufficient for several reflections. In test cases where reflections are not suppressed—such as run 1—the deviation, once it starts, grows rapidly once the reflected wave reaches the cloud interface the first time.

Application of the nonreflecting boundary condition has suppressed the reflected wave and given the physically correct results.

6. Conclusion

A method for obtaining nonreflecting boundary conditions in magnetized, compressible, isothermal inviscid, multi-dimensional fluids has been developed and applied to a 2D case of a rotating, rigid disc (actually a rigid, spherical cloud) with a radial magnetic field, embedded in an external medium of different density and capable of differential rotation. The external medium is initially at rest. The angular velocity of the disc (cloud) changes (decreases) due to the twisting of the field lines at the interface of the cloud and the external medium, giving rise to Alfven waves and converting rotational energy into magnetic energy. The time evolution of the system is followed through numerical modeling of the full fluid equations. The non-

reflecting boundary condition is applied to eliminate spurious reflection of the Alfven waves at the numerical boundary, at the edge of the external medium. The method is applicable to a full 3D model with no simplifying assumptions for the most generalized form of the isothermal fluid equations. In the test case used to verify the method, the run with the nonreflecting boundary condition in place was compared with a run where the external medium was extended to 3 times its original length so that the waves do not get a chance to encounter the numerical boundary during the time period of interest. The results of the two cases match accurately. A comparison run *without* the nonreflecting boundary condition obtains a large deviation of the system in the latter part of the time evolution in comparison with the other cases (where reflection does not occur), showing clear evidence of multiple reflections of the Alfven wave. We believe that this method can be applied to most modeling problems with magnetized, compressible, inviscid fluids and the only exceptions may be cases where the elements of the coefficient matrix are such that they give rise to ill-conditioned matrices of eigenvectors.

Further applications of this method with extensions for handling (real) incoming waves have been completed recently. We have also applied this method to a genuine 2D case of 2-dimensional solar wind models. The models solve the time-dependent MHD equations for a magnetized wind with rotation. The full 3D equations are used with no azimuthal variation. The approach detailed in this paper was successfully applied not only to handle nonreflecting boundary conditions but to treat incoming waves as well. Details of this study will be reported in a subsequent paper.

Appendix: Detailed Equations

The variables to be solved for are the mass density ρ; the r, ϕ, and z components of the velocity (u, v, w); and the magnetic field components (B_r, B_ϕ, B_z). The primitive system of equations corresponding to Eq. (1)–(3) in component form is:

Continuity equation:

$$\frac{\partial \rho}{\partial t} + u\frac{\partial \rho}{\partial r} + \rho\frac{\partial u}{\partial r} + \frac{v}{r}\frac{\partial \rho}{\partial \phi} + \frac{\rho}{r}\frac{\partial v}{\partial \phi} + w\frac{\partial \rho}{\partial z} + \rho\frac{\partial w}{\partial z} + \frac{\rho u}{r} = 0; \tag{45}$$

Navier–Stokes equation:

$$\frac{\partial u}{\partial t} + \frac{c^2}{\rho}\frac{\partial \rho}{\partial r} + u\frac{\partial u}{\partial r} + \frac{B_\phi}{4\pi\rho}\frac{\partial B_\phi}{\partial r} + \frac{B_z}{4\pi\rho}\frac{\partial B_z}{\partial r} + \frac{v}{r}\frac{\partial u}{\partial \phi} - \frac{B_\phi}{4\pi\rho r}\frac{\partial B_r}{\partial \phi} + w\frac{\partial u}{\partial z} - \frac{B_z}{4\pi\rho}\frac{\partial B_r}{\partial z} + \left(\frac{1}{4\pi\rho}\frac{B_\phi^2}{r} - \frac{v^2}{r} - g_r\right) = 0, \tag{46}$$

$$g_r = -\frac{\partial \Phi}{\partial r},$$

$$\frac{\partial v}{\partial t}+u\frac{\partial v}{\partial r}-\frac{B_r}{4\pi\rho}\frac{\partial B_\phi}{\partial r}+\frac{c^2}{\rho r}\frac{\partial \rho}{\partial \phi}+\frac{v}{r}\frac{\partial v}{\partial \phi}+\frac{B_r}{4\pi\rho r}\frac{\partial B_r}{\partial \phi}$$

$$+\frac{B_z}{4\pi\rho r}\frac{\partial B_z}{\partial \phi}+w\frac{\partial v}{\partial z}-\frac{B_z}{4\pi\rho}\frac{\partial B_\phi}{\partial z}+\left(\frac{uv}{r}-\frac{B_rB_\phi}{4\pi\rho r}-g_\phi\right)=0, \tag{47}$$

$$g_\phi=-\frac{1}{r}\frac{\partial \Phi}{\partial \phi},$$

$$\frac{\partial w}{\partial t}+u\frac{\partial w}{\partial r}-\frac{B_r}{4\pi\rho}\frac{\partial B_z}{\partial r}+\frac{v}{r}\frac{\partial w}{\partial \phi}-\frac{B_\phi}{4\pi\rho r}\frac{\partial B_z}{\partial \phi}+\frac{c^2}{\rho}\frac{\partial \rho}{\partial z}$$

$$+w\frac{\partial w}{\partial z}+\frac{B_r}{4\pi\rho}\frac{\partial B_r}{\partial z}+\frac{B_\phi}{4\pi\rho}\frac{\partial B_\phi}{\partial z}-(g_z)=0, \tag{48}$$

$$g_z=-\frac{\partial \Phi}{\partial z};$$

Induction equation:

$$\frac{\partial B_r}{\partial t}-\frac{B_\phi}{r}\frac{\partial u}{\partial \phi}+\frac{B_r}{r}\frac{\partial v}{\partial \phi}+\frac{v}{r}\frac{\partial B_r}{\partial \phi}-\frac{u}{r}\frac{\partial B_\phi}{\partial \phi}-B_z\frac{\partial u}{\partial z}$$

$$+B_r\frac{\partial w}{\partial z}+w\frac{\partial B_r}{\partial z}-u\frac{\partial B_z}{\partial z}=0, \tag{49}$$

$$\frac{\partial B_\phi}{\partial t}+B_\phi\frac{\partial u}{\partial r}-B_r\frac{\partial v}{\partial r}-v\frac{\partial B_r}{\partial r}+u\frac{\partial B_\phi}{\partial r}-B_z\frac{\partial v}{\partial z}$$

$$+w\frac{\partial B_\phi}{\partial z}+B_\phi\frac{\partial w}{\partial z}-v\frac{\partial B_z}{\partial z}=0, \tag{50}$$

$$\frac{\partial B_z}{\partial t}+B_z\frac{\partial u}{\partial r}-B_r\frac{\partial w}{\partial r}-w\frac{\partial B_r}{\partial r}+u\frac{\partial B_z}{\partial r}+\frac{B_z}{r}\frac{\partial v}{\partial \phi}$$

$$-\frac{B_\phi}{r}\frac{\partial w}{\partial \phi}-\frac{w}{r}\frac{\partial B_\phi}{\partial \phi}+\frac{v}{r}\frac{\partial B_z}{\partial \phi}+\left(\frac{uB_z}{r}-\frac{wB_r}{r}\right)=0. \tag{51}$$

For the r direction Eq. (49) does not contribute to the matrix **A**, because this equation does not have $\partial \mathbf{U}/\partial r$ terms. Therefore it is evaluated with ordinary finite difference formulas at the r boundaries. For the z direction Eq. (51) is left out of the matrix for the same reason.

For the z direction $\mathbf{U}$ and $\mathbf{A}$ are

$$\mathbf{U}=\begin{pmatrix}\rho\\ u\\ v\\ w\\ B_r\\ B_\phi\end{pmatrix},\qquad \mathbf{A}=\begin{pmatrix} w & 0 & 0 & \rho & 0 & 0\\ 0 & w & 0 & 0 & \dfrac{-B_z}{4\pi\rho} & 0\\ 0 & 0 & w & 0 & 0 & \dfrac{-B_z}{4\pi\rho}\\ \dfrac{c^2}{\rho} & 0 & 0 & w & \dfrac{B_r}{4\pi\rho} & \dfrac{B_\phi}{4\pi\rho}\\ 0 & -B_z & 0 & B_r & w & 0\\ 0 & 0 & -B_z & B_\phi & 0 & w\end{pmatrix}, \tag{52}$$

and the symmetrized matrix $\mathbf{A}'$ ($\equiv\mathbf{D}^{-1}\mathbf{A}\mathbf{D}$) is

$$\mathbf{A}'=\begin{pmatrix} w & 0 & 0 & c & 0 & 0\\ 0 & w & 0 & 0 & \dfrac{-B_z}{\sqrt{4\pi\rho}} & 0\\ 0 & 0 & w & 0 & 0 & \dfrac{-B_z}{\sqrt{4\pi\rho}}\\ c & 0 & 0 & w & \dfrac{B_r}{\sqrt{4\pi\rho}} & \dfrac{B_\phi}{\sqrt{4\pi\rho}}\\ 0 & \dfrac{-B_z}{\sqrt{4\pi\rho}} & 0 & \dfrac{B_r}{\sqrt{4\pi\rho}} & w & 0\\ 0 & 0 & \dfrac{-B_z}{\sqrt{4\pi\rho}} & \dfrac{B_\phi}{\sqrt{4\pi\rho}} & 0 & w\end{pmatrix}. \tag{53}$$

The diagonal elements of the symmetrizing matrix $\mathbf{D}$ and its inverse are the same as for the r direction.

ACKNOWLEDGMENTS

One of the authors (TCV) would like to thank John Avila from the Cray User Services department at NASA Ames Research Center for his extensive help in developing the semi-analytic approach and the interest he showed in the research. Thanks are also due to Drs. Aaron Barnes and Paul Gazis for instructive discussions. This research was supported by National Research Council Research Associateships for both TCV and KWT.

REFERENCES

1. K. W. THOMPSON, *J. Comput. Phys.* **68**, 1 (1987).
2. T. CH. MOUSCHOVIAS, *Astrophys. J.* **230**, 204 (1979).